Fig. 9. With the exception of one smaller ripple and slower rate of cutoff at 3 GHz–30-dB region, the experimental result is in very close agreement with the theoretical prediction shown in Fig. 7.

VII. Coupled Filters

The design equations of Table I can be modified to include coupled filters such as those shown in Fig. 10. This can be done readily by the graphical transformation technique [12], and the results are presented in Tables II and III.

VIII. Conclusion

The design formulas presented in Tables I–III have the following advantages over other existing approximate design formulas.

1) The new design formulas are simpler.

2) Two fewer sections are required for the parallel-coupled filters.

3) The identical coupling parameters (Y_0) in the filter structure may offer some mechanical advantages in the physical realization of the filter.

4) The worst VSWR of the filter in the passband can be predicted (4) and precorrected if necessary.

The comparative ease with which these new design equations were derived also demonstrated the effectiveness of the new approach presented in the companion paper [7].

Acknowledgment

The author wishes to thank the reviewers for their helpful suggestions.

References

[1] S. B. Cohn, "Parallel-coupled transmission-line-resonator filters," *IRE Trans. Microwave Theory Tech.*, vol. MTT-6, pp. 223–231, Apr. 1958.
[2] G. L. Matthaei, "Design of wide-band (and narrow-band) band-pass microwave filters on the insertion loss basis," *IRE Trans. Microwave Theory Tech.*, vol. MTT-8, pp. 580–593, Nov. 1960.
[3] E. G. Cristal, "New design equations for a class of microwave filters," *IEEE Trans. Microwave Theory Tech.* (Corresp.), vol. MTT-19, pp. 486–490, May 1971.
[4] R. J. Wenzel, "Exact theory of interdigital band-pass filters and related coupled structures," *IEEE Trans. Microwave Theory Tech. (Special Issue on Microwave Filters)*, vol. MTT-13, pp. 559–575, Sept. 1965.
[5] W. W. Mumford, "Tables of stub admittances for maximally flat filters using shorted quarter-wave stubs," *IEEE Trans. Microwave Theory Tech.* (Corresp.), vol. MTT-13, pp. 695–696, Sept. 1965.
[6] M. Dishal, "A simple design procedure for small percentage bandwidth round-rod interdigital filters," *IEEE Trans. Microwave Theory Tech.* (Corresp.), vol. MTT-13, pp. 696–698, Sept. 1965.
[7] K. K. Pang, "Normal transmission-line networks and their lumped *LC* presentation," this issue, pp. 601–607.
[8] E. G. Cristal, "A frequency transformation for commensurate transmission-line networks," *IEEE Trans. Microwave Theory Tech.*, vol. MTT-15, pp. 348–357, June 1967.
[9] A. Matsumoto, *Microwave Filter and Circuits, Advances in Microwave Series*. New York: Academic Press, 1970. ch. VI, p. 176.
[10] D. C. Youla, "A tutorial exposition of some key network-theoretic ideas underlying classical insertion-loss filter design," *Proc. IEEE*, vol. 59, pp. 760–799, May 1971.
[11] D. C. Youla and P. M. Paterno, "Realizable limits of error for dissipationless attenuators in mismatched systems," *IEEE Trans. Microwave Theory Tech.*, vol. MTT-12, pp. 289–299, May 1964.
[12] R. Sato and E. G. Cristal, "Simplified analysis of coupled transmission-line networks," *IEEE Trans. Microwave Theory Tech.*, vol. MTT-18, pp. 122–131, Mar. 1970.
[13] L. Weinberg, *Network Analysis and Synthesis*. New York: McGraw-Hill, 1962, p. 607.
[14] M. Sucher and J. Fox, *Handbook of Microwave Measurements*, vol. 1. New York: Wiley, 1963, p. 369.
[15] D. J. Wilde and C. S. Beightler, *Foundations of Optimization*. Englewood Cliffs, N. J.: Prentice-Hall, 1967, ch. 3.

Design of Acoustic Surface-Wave Devices Using an Admittance Formalism

ALAN S. BURGESS AND PETER H. COLE

***Abstract*—The advantages of an admittance formalism for the derivation of performance characteristics of transversal filters and one-port information stores using acoustic surface-wave delay lines are described. An expression for the transadmittance between transducer pairs in the weak-coupling approximation is derived using a normal mode theory. The formulation is found to give good agreement with measurements of the passband response of a wide-band logarithmically frequency-tapered transducer pair on *YX*-quartz A brief discussion of the limitations of the model is included.**

Manuscript received September 12, 1972; revised January 29, 1973, and June 6, 1973.

A. S. Burgess is with the Department of Electrical Engineering, University of Adelaide, S. Aust., 5001, Australia.

P. H. Cole is with the School of Electrical Engineering, University of Sydney, N.S.W., 2006, Australia.

I. Introduction

THE ART of signal processing by means of acoustic surface-wave devices depends in large measure on the exploitation of the characteristics of multitapped delay lines in the synthesis of two-port transversal filters. Multitap delay lines in which all the transducers are connected in parallel to form a one-port device also find application in the field of information storage and encoding in that they are one-port

passive elements which will return an information-bearing reply signal in the form of a pulse code in the time domain in response to interrogation by a short pulse.

The principal parameters of interest to the users of such devices are the input immittances and voltage transfer ratios for the two-port structures and the time-domain response for one-port structures. There are several methods available for calculating the input immittance for a single transducer, including the empirical three-port model of Smith *et al.* [1], the integral formulation of Auld and Kino [2] based on a normal mode analysis, and the variational method described by Milsom and Redwood [3]. For the calculation of the voltage transfer ratio, the three-port model of Smith *et al.* may be used although the calculation is rather complex. Tancrell and Holland [4] and Morgan [5] have shown how the three-port model can be applied to the determination of the responses of apodized transducer structures. More recently, the three-port model has been extended by Smith *et al.* [6] and Jones *et al.* [7] to enable the prediction of second-order effects on strong coupling substrates, the most important of which are regeneration, and reflection from the acoustic mismatch between the metallized and unmetallized regions within a transducer.

The structures which were discussed above, namely transversal filters and one-port information stores, possess the common property of parallel connection of many surface-wave transducers and, as will be shown, this property renders an admittance formulation extremely useful in predicting their characteristics. Both the input immittance and the voltage transfer ratios may be related in a direct manner to the properties of an admittance matrix of the structure in either the time or frequency domain.

Auld and Kino [2] have described a method for the calculation of the input immittance of a single transducer, at least in the weak-coupling approximation, which is appropriate to most materials on which multitap devices are fabricated, by a normal mode theory. In this paper the normal mode theory is extended to produce an expression for the transfer admittance between a pair of transducers, again on weak-coupling substrates. Thus it becomes practical to propose the admittance formalism as a complete and convenient method for characterizing surface acoustic-wave devices with any number of electrical ports.

Section II of this paper will deal with the utilization of an admittance formulation in the determination of quantities of interest in tapped delay lines and one-port information stores, while Section III will present a normal mode theory for the calculation of transfer admittances in the weak-coupling approximation. Experimental measurements will be presented in Section IV for comparison with the calculations as applied to a wide-band delay line structure, and the paper concludes with a discussion, in Section V, of the limitations of the methods used.

II. The Admittance Formulation

The admittance matrix for a two-port delay line is defined by the equation

$$\begin{bmatrix} \dot{I}_1 \\ \dot{I}_2 \end{bmatrix} = \begin{bmatrix} Y_{11} & Y_{12} \\ Y_{21} & Y_{22} \end{bmatrix} \begin{bmatrix} \dot{V}_1 \\ \dot{V}_2 \end{bmatrix} \tag{1}$$

in which $\dot{V}_i$ and $\dot{I}_i$ are complex phasors representing the peak values of terminal voltages and currents with the senses shown in Fig. 1, and Y_{ij} are complex functions of frequency. A knowledge of the admittance matrix at all frequencies provides a complete characterization of the delay line.

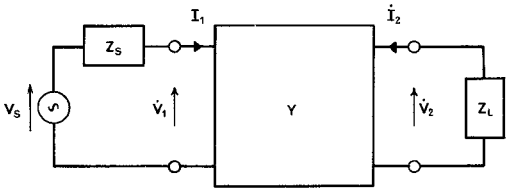

Fig. 1. Equivalent circuit of a two-port surface-wave delay line connected between a source of impedance Z_S and a load impedance Z_L.

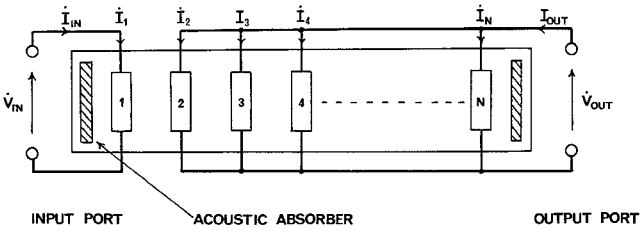

Fig. 2. Circuit showing the external electrical connections of an N-port delay line connected as a transversal filter.

The quantity of most common interest to a filter designer is the voltage transfer ratio to be expected when the line is connected between a signal generator of source impedance Z_S and a load of impedance Z_L, as shown in the equivalent circuit of Fig. 1. This ratio is given by

$$\frac{\dot{V}_L}{\dot{V}_S} = \frac{-Y_{21}Z_L}{1+Y_{11}Z_S+Y_{22}Z_L+Z_SZ_L(Y_{11}Y_{22}-Y_{12}Y_{21})}. \tag{2}$$

When a weak-coupling substrate is employed in a filter which is to be inserted without impedance matching into a 50-Ω system, the source and load impedances are real, and the inequalities

$$\begin{aligned} |Y_{11}|R_S &\approx |Y_{22}|R_L \ll 1 \\ |Y_{21}|R_S &= |Y_{12}|R_L \ll 1 \end{aligned} \tag{3}$$

usually hold.

In this case the voltage transfer ratio simplifies to

$$\frac{\dot{V}_L}{\dot{V}_S} = -Y_{21}(\omega)R_L \tag{4}$$

which shows that the voltage transfer ratio between the input and output ports of a delay line is determined simply by the product of the transadmittance between the input and output ports and the load impedance, with an accuracy dependent only on the validity of the approximations in (3). The practical significance of this result is that measurement in such unmatched systems provides an accurate and direct experimental check on the form of the transadmittance function, which is the most important system design parameter.

The admittance formalism is also of particular convenience for use in predicting the behavior of acoustic surface-wave lines with multiple transducers in the propagation path connected to a small number of external electrical ports. Consider, for example, the equivalent circuit for the transversal filter shown in Fig. 2. If we first determine the admittance matrix Y_{ij} $(i, j=1 \cdots N)$ for the delay line, treating the device as an N-port, then it is a straightforward matter to show that the network equations for the resulting two-port take the form

$$\begin{bmatrix} \dot{I}_{\text{in}} \\ \dot{I}_{\text{out}} \end{bmatrix} = \begin{bmatrix} Y_{11}' & Y_{12}' \\ Y_{21}' & Y_{22}' \end{bmatrix} \begin{bmatrix} \dot{V}_{\text{in}} \\ \dot{V}_{\text{out}} \end{bmatrix} \tag{5}$$

in which the elements of the new admittance matrix given by

$$Y_{11}' = Y_{11} \qquad Y_{12}' = \sum_{i=2}^{N} Y_{1i}$$

$$Y_{21}' = \sum_{i=2}^{N} Y_{i1} \qquad Y_{22}' = \sum_{i=2}^{N}\sum_{j=2}^{N} Y_{ij} \tag{6}$$

may be seen to be simple sums of the admittance elements of the N-port. This property of the admittance formalism is a consequence of the parallel connection of the delay line taps.

The usefulness of an admittance formalism is not limited to unmatched source and load conditions. If the approximations involved in simplifying (2) are not justified, as would be the case with impedance-matched transducers or with moderate to strong coupling substrates, then (4) cannot be used. A common problem which arises in such cases in the design of signal-processing lines and filters is the prediction of the triple-transit signal. In the admittance formulation this can be done quite simply by manipulation of (2). If the input admittance terms Y_{11} and Y_{22} can be treated as constants over the frequency range of interest, then (2) can be rewritten in the form

$$\frac{\dot{V}_L}{\dot{V}_S} = \frac{-A\,Y_{21}R_L}{1 - AR_SR_LY_{12}Y_{21}} \tag{7}$$

where $A = [(1+Y_{11}R_S)(1+Y_{22}R_L)]^{-1}$. Provided $B = AR_SR_LY_{12}Y_{21}$ has magnitude less than unity, (7) can be expanded by the binomial theorem to give

$$\dot{V}_L = -AY_{21}R_L\dot{V}_S[1 - B + B^2 - B^3 \cdots]. \tag{8}$$

Taking the Fourier transform of both sides to observe the time-domain response, we obtain

$$v_L(t) = -v_S(t)*y_{21}'(t)+v_S(t)*y_{21}'(t)*y_{12}'(t)*y_{21}'(t)- \cdots \tag{9}$$

where

$$y_{21}'(t) = Ay_{21}(t)R_L$$
$$y_{12}'(t) = y_{12}(t)R_S$$

and * indicates convolution.

Comparison of this expression with (4) shows that the first term in the expansion corresponds to the primary response of the line; $y_{21}'(t)$ is the primary impulse response of the delay line when excited at port 1, and similarly for $y_{12}'(t)$. The second term of the expansion gives the time-domain response due to the triple-transit signal, and subsequent terms give the higher order reflections which are normally of little interest due to their greater attenuation.

The effects resulting from the variable input impedance of the transducers can also be predicted from (2). It can be seen that an increase in the magnitude of Y_{11} and Y_{22} at any frequency will result in a reduction of the ratio $\dot{V}_L/\dot{V}_S$. One consequence of this is that the launching of volume waves in a line, even if not detected by the receiving transducer, will still affect $\dot{V}_L/\dot{V}_S$ through the variation of Y_{11} and Y_{22}.

Another device for which the admittance formalism is of particular utility is the one-port echo line, shown in Fig. 3(a). Devices of this type have been studied by the authors for their use in information encoding and storage, as it is possible to construct a series of lines of varying patterns in which each line responds to an input pulse with a unique train of echo pulses coded in the time domain.

The equivalent circuit for a one-port line, connected to a source and receiver, is shown in Fig. 3(b). To predict the

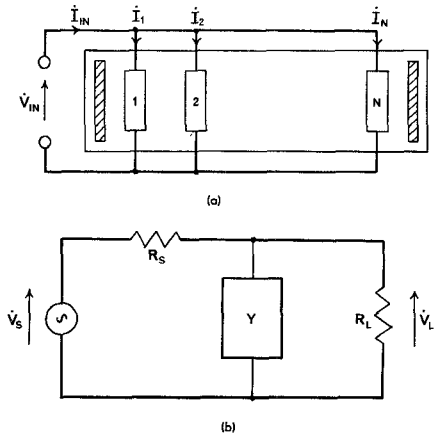

Fig. 3. Equivalent circuits for a one-port echo line showing (a) transducer interconnections and (b) measurement circuit.

response of such a line, which may have many transducers connected in parallel, it is again necessary to evaluate the elements of the N-port admittance matrix. The total input admittance is then given by

$$Y = \sum_{i=1}^{N}\sum_{j=1}^{N} Y_{ij} \tag{10}$$

and the voltage transfer ratio is given by

$$\frac{\dot{V}_L}{\dot{V}_S} = \frac{1}{1 + \dfrac{R_S}{R_L} + R_SY}. \tag{11}$$

If we substitute Y_a+jB_0 for Y, where $jB_0=j\omega C_T$ is the susceptance of the static transducer capacitance, the voltage transfer ratio becomes

$$\frac{\dot{V}_L}{\dot{V}_S} = \frac{Z}{R_S(1 + ZY_a)} \tag{12}$$

where $Z=R_SR_L[R_S+R_L+R_SR_LjB_0]^{-1}$ is the impedance of R_S, R_L, and the transducer capacitance all in parallel. Normally $|ZY_a| < 1$ and we can write

$$\dot{V}_L=\dot{V}_SZ(R_S)^{-1}[1-ZY_a+(ZY_a)^2-(ZY_a)^3+ \cdots]. \tag{13}$$

If we take the Fourier transform of both sides, we can observe the time response of the line

$$v_L(t) = v_S'(t) - v_S'(t)*y'(t) + v_S'(t)*y'(t)*y'(t) \cdots \tag{14}$$

where $v_S'(t)=v_S(t)*z(t)(R_S)^{-1}$ and $y'(t)=z(t)*y_a(t)$. The first term of the expansion represents the source voltage as seen by the line, which would be a short pulse in a practical system. The principal response of interest is given by the second term, which provides the primary echo response of the system, $y'(t)$ being regarded as the primary impulse response of the line. The subsequent terms represent the higher order responses, i.e., echoes excited by earlier echoes. These are normally neglected because $|y'(t)|$ is much less than unity, but can be evaluated in situations where it is thought that subsequent responses might produce unacceptable interference with the main replay signal.

In order to apply the admittance formalism discussed in this section to practical problems, methods for the calculation of input admittances of single transducers and transfer admittances between transducers must be available. The calculation of input admittances by normal mode theory [2]

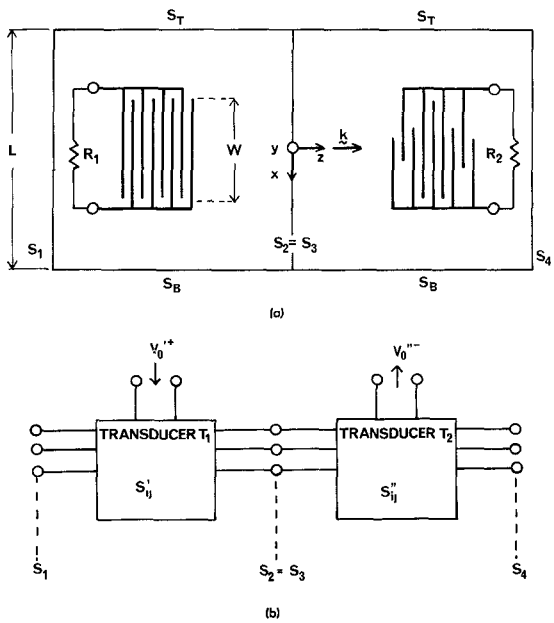

Fig. 4. Two-transducer structure. (a) Schematic showing coordinate system and boundary surfaces referred to in text. (b) Scattering matrix representation for normal modes.

was mentioned earlier. It is the purpose of the next section to describe a normal mode theory for the calculation of transfer admittances between pairs of transducers on a weak-coupling substrate. The transadmittance is derived for a pair of transducers separated by a length of free substrate surface, but the formula can also usefully be applied to transducers on a multitap delay line in situations where the reflections from the intermediate transducers, which are short circuited in the admittance calculation, are much less than the regeneration effects which these transducers present at their working load impedances.

III. Derivation of Transadmittance

The system for which we derive an expression for the transadmittance is shown in Fig. 4(a), in which the transadmittance Y_{21} between a transducer T_1 of uniform width W and an apodized transducer T_2 of maximum width $<W$ is to be determined. The calculation is facilitated by making the artificial assumption that the configuration is repeated periodically along the x axis with some large periodicity interval L; the principal effect of this assumption is the introduction of an artificial discrete set of normal modes. These modes are obtained by using linear combinations of straight-crested surface waves to satisfy the periodic boundary conditions at $x = \pm L/2$. In this way one obtains modal fields whose components are trigonometric functions of all the integer multiples of $2\pi x/L$. We will adopt a mode-labeling scheme such that a mode with positive index m propagates to the right in Fig. 4, while a mode with negative index $-m$ propagates in the opposite direction.[1] The zero mode index will be reserved for signals at the electrical ports of one or the other of the transducers. If one assumes that reference planes S_1, $S_2 = S_3$, and S_4 in the figure are sufficiently far from the transducers for the nonpropagating modes to have decayed to negligible amplitude, we need consider only the propagating modes. At a particular frequency ω there will be a finite number $2N$ of such modes.

As a further consequence of the periodic boundary conditions, it may be shown that the field vectors of the propagating acoustic surface-wave normal modes satisfy the orthogonality relations [8]

$$\int_S (-j\omega\phi_m \boldsymbol{D}_n^* + j\omega\phi_n^* \boldsymbol{D}_m - \boldsymbol{v}_m \cdot \tilde{\boldsymbol{T}}_n^* - \boldsymbol{v}_n^* \cdot \tilde{\boldsymbol{T}}_m) \cdot \boldsymbol{k}\, dS = \begin{cases} 0 & \text{when } m \neq n \\ 4P_n & \text{when } m = n \end{cases} \quad (15)$$

where $\phi_m(x, y, z)$, $\boldsymbol{D}_m(x, y, z)$, $\boldsymbol{v}_m(x, y, z)$, and $\tilde{\boldsymbol{T}}_m(x, y, z)$ are complex phasors representing peak values of potential, electric displacement, particle velocity, and stress tensor of normal mode m, and S is any one of the surfaces S_1, $S_2 = S_3$, or S_4 perpendicular to the z axis shown in Fig. 4(a), and extending from $y=0$ to $y \to +\infty$ over the interval $-L/2 < x < L/2$. The power P_m is the power carried to the right by normal mode m. In our mode-labeling scheme for which $\beta_m = -\beta_{-m}$, we have also $P_m = -P_{-m}$. Selecting a common value P for which $P_m = P$ for $m > 0$ and $P_m = -P$ for $m < 0$ will normalize the fields ϕ_m, $\boldsymbol{D}_m$, etc., to definite values.

Since the nonpropagating modes are assumed to be of negligible amplitude at the reference plane $S_2 = S_3$, we may express the field at this point in the form

$$\begin{aligned} \phi &= \sum_{m=-1}^{-N} V_m^{(2)} \phi_m + \sum_{m=1}^{N} V_m^{(2)} \phi_m \\ \boldsymbol{D} &= \sum_{m=-1}^{-N} V_m^{(2)} \boldsymbol{D}_m + \sum_{m=1}^{N} V_m^{(2)} \boldsymbol{D}_m \\ \tilde{\boldsymbol{T}} &= \sum_{m=-1}^{-N} V_m^{(2)} \tilde{\boldsymbol{T}}_m + \sum_{m=1}^{N} V_m^{(2)} \tilde{\boldsymbol{T}}_m \\ \boldsymbol{v} &= \sum_{m=-1}^{-N} V_m^{(2)} \boldsymbol{v}_m + \sum_{m=1}^{N} V_m^{(2)} \boldsymbol{v}_m. \end{aligned} \quad (16)$$

The coefficients $V_m^{(2)}$ may be regarded as complex generalized voltage amplitudes of forward and backward waves which enter ($m<0$) or leave ($m>0$) transducer T_1 through a series of N acoustic surface-wave ports which have a common reference plane S_2. If we adopt the notation $V_0'^+$ and $V_0'^-$ for the input and output generalized voltage waves at the electrical port of T_1, we may write, on the assumption that no signals enter T_1 across the plane S_1, the scattering matrix equation

$$\begin{bmatrix} V_0'^- \\ V_1^{(2)} \\ V_2^{(2)} \\ \vdots \\ V_N^{(2)} \end{bmatrix} = \begin{bmatrix} S_{00}', S_{0-1}', S_{0-2}', \cdots S_{0-N}' \\ S_{10}', S_{1-1}', \quad \cdots \quad S_{1-N}' \\ \vdots \quad\quad\quad\quad\quad \vdots \\ S_{N0}' \quad\quad \cdots \quad\quad S_{N-N}' \end{bmatrix} \begin{bmatrix} V_0'^+ \\ V_{-1}^{(2)} \\ V_{-2}^{(2)} \\ \vdots \\ V_{-N}^{(2)} \end{bmatrix} \quad (17)$$

in which the assignment of mode numbers has produced symmetry of the matrix in the form $S_{i0}' = S_{0-i}'$. A requirement for symmetry of the scattering matrix is that all generalized voltages are defined in a way that unit amplitude waves carry a common power P. This requirement has already been satisfied at the acoustic ports. To facilitate its adoption at the electrical ports, the normal transducer structures of T_1 and T_2 have been supplemented in Fig. 4(a) by the parallel-con-

[1] In this mode-labeling scheme, modes with equal z- and oppositely directed x-propagation constants are associated with different mode numbers.

nected low-value resistors R_1 and R_2, which are chosen to have a resistance much less than the input impedances of T_1 and T_2, so that T_1 and T_2 can be regarded as matched when fed from transmission lines for which R_1 and R_2 are the respective characteristic impedances. A consequence of these restrictions is that the actual voltage $\dot{V}$ between the fingers of transducer T_1 will be related to the incident generalized voltage amplitude by

$$\dot{V} = V_0'^{+}\sqrt{2PR_1}. \tag{18}$$

It will be seen later, from (39), that the transadmittance from T_1 to T_2 is independent of the choice of resistors R_1 and R_2.

The set of normal modes which communicate with transducer T_2, assuming that no signals enter T_2 from across S_4, are those which cross S_3. If these are assigned mode amplitudes $V_m^{(3)}$, ($m>0$, input modes and $m<0$, output modes), and the input and output waves at the electrical port have the respective amplitudes $V_0''^{+}$ and $V_0''^{-}$, the scattering matrix equation for T_2 takes the form

$$\begin{bmatrix} V_0''^{-} \\ V_{-1}^{(3)} \\ V_{-2}^{(3)} \\ V_{-3}^{(3)} \\ \vdots \\ V_{-N}^{(3)} \end{bmatrix} = \begin{bmatrix} S_{00}'', S_{01}'', S_{02}'' \cdots S_{0N}'' \\ S_{-10}'', \quad \cdots \quad S_{-1N}'' \\ S_{-20}'', \quad \cdots \\ \vdots \qquad\qquad \vdots \\ S_{-N0}'', \quad \cdots \quad S_{-NN}'' \end{bmatrix} \begin{bmatrix} V_0''^{+} \\ V_1^{(3)} \\ V_2^{(3)} \\ V_3^{(3)} \\ \vdots \\ V_N^{(3)} \end{bmatrix} \tag{19}$$

in which the assignment of mode numbers adopted has produced symmetry in the form $S_{-i0}'' = S_{0i}''$.

The connection between transducers T_1 and T_2 arises because the output modes of T_1 become the input modes of T_2 on the common reference plane $S_2 = S_3$, as shown in Fig. 4(b). Thus we obtain the equation $V_m^{(2)} = V_m^{(3)}$ for all $m>0$. Suppose that T_1 is excited with an incident voltage $V_0'^{+}$ and that T_2 is terminated in a matched load R_2. The latter condition means that $V_0''^{+}=0$ in (19). It is, furthermore, assumed that the acoustic scattering at T_2 is negligible when the electrical port is short circuited.[2] In this case $V_{-m}^{(2)} = V_{-m}^{(3)} = 0$ in (17) and (19), and it is found that

$$\frac{V_0''^{-}}{V_0'^{+}} = \sum_{i=1}^{N} S_{0i}''S_{i0}' = \sum_{i=1}^{N} S_{-i0}''S_{i0}' \tag{20}$$

in which the symmetry of $\tilde{\mathbf{S}}''$ has been used. For further progress, explicit expressions for the scattering matrix elements, which may be derived from a knowledge of the normal mode amplitudes launched by known source distributions on T_1 or T_2, are required.

The calculation of the amplitude of a normal mode field launched by a known source distribution on transducer T_1 proceeds from consideration of the complex reciprocity integral

$$\int_S (-j\omega\phi_s \boldsymbol{D}_m^* + j\omega\phi_m^* \boldsymbol{D}_s - \boldsymbol{v}_s \cdot \tilde{\boldsymbol{T}}_m^* - \boldsymbol{v}_m^* \cdot \tilde{\boldsymbol{T}}_s) \cdot d\boldsymbol{S} = 0 \tag{21}$$

established by Auld [8] for a lossless piezoelectric medium in which no free charges or body forces are present. In the above integral ϕ_s, $\boldsymbol{D}_s$, etc., is the total field launched by a particular source distribution at frequency ω. ϕ_m, $\boldsymbol{D}_m$, etc., is the field of a normal mode at the same frequency ω, and $d\boldsymbol{S}$ is an element of area directed outward from a closed surface S which we will choose in the present case to consist of the propagation surface of the substrate, the boundary surfaces S_1, S_2, S_T, and S_B in Fig. 4, and a plane deep in the material. On the assumption that on planes S_1 and S_2 the propagating normal modes form a complete set for expansion of the fields ϕ_s, $\boldsymbol{D}_s$, etc., launched by the sources, and making use of the orthogonality relations (15), we may derive the expression for the amplitude of normal mode m,

$$V_m^{(2)} = \frac{-1}{4P}\int_{S'} [-j\omega\phi_s \boldsymbol{D}_m^* + j\omega \boldsymbol{D}_s\phi_m^*] \cdot d\boldsymbol{S} \tag{22}$$

where the integration is over the surface S' of transducer T_1, $d\boldsymbol{S}$ is directed upward, and mode m has $m>0$. The displacement vectors for the source field and the Rayleigh normal mode field can be eliminated from this expression to obtain

$$V_m^{(2)} = \frac{j\omega}{4P}\int_{S'} [\epsilon_0\beta_m\phi_s + \sigma_s]\phi_m^* \, dS \tag{23}$$

where σ_s is the charge density on the underside of a finger, ϕ_s is the electrostatic potential established at the substrate surface by the source distribution, and we have used the fact that for a Rayleigh wave of propagation constant β_m, of magnitude β_m, the normal component of electric flux density is related to the potential by

$$\boldsymbol{D}_m \cdot d\boldsymbol{S} = \epsilon_0 \beta_m \phi_m \, dS$$

for all propagation directions in the xz plane. At this point we make the assumption that the variation in propagation velocity with direction on the substrate can be neglected, and we replace β_m by a constant value β.

Equation (23) can be condensed somewhat by the definition of a source function $f'(x, z)$ for a transducer pattern operated at a particular frequency by the relation

$$\epsilon_0\dot{V}f'(x, z) = \sigma_s(x, 0, z) + \epsilon_0\beta\phi_s(x, 0, z). \tag{24}$$

The amplitude of a normal mode m launched toward reference plane S_2 then becomes

$$V_m^{(2)} = \frac{j\omega\epsilon_0\dot{V}}{4P}\int_{S'} f'(x, z)\phi_m^*(x, z) \, dS. \tag{25}$$

If we make use of (18) to eliminate $\dot{V}$, the result is the equation for the scattering matrix element

$$S_{i0}' = \frac{j\omega\epsilon_0\sqrt{2PR_1}}{4P}\int_{S'} f'(x, z)\phi_i^*(x, z) \, dS. \tag{26}$$

A similar equation may be deduced for S_{-i0}'', viz.

$$S_{-i0}'' = \frac{j\omega\epsilon_0\sqrt{2PR_2}}{4P}\int_{S''} f''(x, z)\phi_{-i}^*(x, z) \, dS. \tag{27}$$

The voltage ratio (20) may now be written

$$\frac{V_0''^{-}}{V_0'^{+}} = \frac{-\omega^2\epsilon_0^2\sqrt{R_1R_2}}{8P}\sum_{i=1}^{N}\int_{S'} \phi_i^*(x, z)f'(x, z) \, dS \int_{S''} \phi_{-i}^*(x, z)f''(x, z)dS. \tag{28}$$

We now interchange the order of summing and forming the

[2] This is not a satisfactory approximation for strong-coupling substrates.

second projection, and make use of the result $\phi_{-i}^*(x,z) = \phi_i(x,z)$, which follows if we adopt (without loss of generality) the convention $\phi_i(0,0) = \phi_i^*(0,0)$ for all normal modes. The voltage transfer equation (28) then becomes

$$\frac{V_0''^-}{V_0'^+} = \frac{-\omega^2\epsilon_0^2\sqrt{R_1R_2}}{8P} \cdot \int_{S''}\left[\sum_{i=1}^{N}\int_{S'}\phi_i^*(x,z)f'(x,z)\,dS\right]\phi_i(x,z)f''(x,z)\,dS. \quad (29)$$

In view of the normal mode expansion (16) and the expressions for normal mode amplitudes (25), the coefficient of $f''(x, z)$ in the integral can be recognized (apart from a constant factor) as the total field, which we will call $\phi(x, z)$, radiated by transducer T_1 towards the region of transducer T_2. Thus we obtain

$$\frac{V_0''^-}{V_0'^+} = \frac{j\omega\epsilon_0\sqrt{2PR_2}}{4P}\int_{S''}\phi(x,z)f''(x,z)\,dS. \quad (30)$$

This expression allows for the effects of diffraction in the field launched by transducer T_1. We will now assume, however, that at all frequencies of interest, the width W of transducer T_1 is $\gg\lambda$, so that its radiated field $\phi(x, z)$ in the vicinity of transducer T_2 is essentially the uniform plane wave

$$\phi(x,z) = \phi(0,0)e^{-j\beta z}, \qquad \frac{-W}{2} < x < \frac{W}{2} \quad (31)$$

where β is the propagation vector at frequency ω in the z direction on the unperturbed substrate. The coefficient $\phi(0, 0)$ can be related to the driving amplitude $V_0'^+$ by invoking conservation of power between the field $\phi(x, z)$ and the set of normal modes $\phi_i(x, z)$ into which it can be decomposed.

The power carried in width W by a uniform plane wave is given in terms of the surface-wave potential ϕ and the commonly accepted measure Δ of piezoelectric coupling for surface waves by Ingebrigtsen's [9] perturbation formula as

$$\boldsymbol{P} = -\,|\omega|W(\epsilon_0+\epsilon_p)\,|\,\phi(0,0)\,|^2/(4\Delta) \quad (32)$$

where ϵ_p is the effective permittivity of the substrate and Δ is the fractional change in surface-wave velocity between a free and a metallized propagating surface. The power $\boldsymbol{P}$ is also given in terms of the normal mode amplitudes by the equation

$$\boldsymbol{P} = \sum_{i=1}^{N} V_i^{(2)}V_i^{(2)*} \quad (33)$$

which, after substitution for $V_i^{(2)}$ from (25) and interchange of order of summation and integration, becomes

$$\boldsymbol{P} = \frac{j\omega\epsilon_0 V_0'^+\sqrt{2PR_1}}{4}\int_{S'}f'(x,z)\sum_{i=1}^{N}V_i^{(2)*}\phi_i^*(x,z)\,dS = \frac{j\omega\epsilon_0 V_0'^+\sqrt{2PR_1}}{4}\phi^*(0,0)\int_{S'}f'(x,z)e^{j\beta z}\,dS. \quad (34)$$

Equating the two values of $\boldsymbol{P}$ obtained gives

$$\phi(0,0) = \frac{-j\omega\Delta\epsilon_0 V_0'^+\sqrt{2PR_1}}{|\omega|\,W(\epsilon_0+\epsilon_p)}\int_{S'}f'(x,z)e^{j\beta z}\,dS. \quad (35)$$

We may now substitute for $\phi(x, z) = \phi(0, 0)e^{-j\beta z}$ in (30) for the output of transducer T_2 and obtain

$$\frac{V_0''^-}{V_0'^+} = \frac{|\omega|\Delta\epsilon_0^2\sqrt{R_1R_2}}{2W(\epsilon_0+\epsilon_p)}[F_1][F_2] \quad (36)$$

where we have introduced F_1 and F_2 defined by

$$F_1 = \int_{S'}f'(x,z)e^{j\beta z}\,dS$$

$$F_2 = \int_{S''}f''(x,z)e^{-j\beta z}\,dS. \quad (37)$$

To calculate the transadmittance we must relate the voltage $\dot{V}$ on transducer T_1 to $V_0'^+$ by (18), and the short-circuit current $\dot{I}$ in transducer T_2 to $V_0''^-$ by the relation

$$\dot{I} = -\,2V_0''^-\sqrt{2P/R_2}. \quad (38)$$

The short-circuit forward transadmittance $Y_{21}(\omega) = \dot{I}/\dot{V}$ then becomes, from (36)

$$Y_{21}(\omega) = \frac{-|\omega|\Delta\epsilon_0^2}{W(\epsilon_0+\epsilon_p)}\int_{S'}f'(x,z)e^{j\beta z}\,dS \int_{S''}f''(x,z)e^{-j\beta z}\,dS. \quad (39)$$

Since the forward transadmittance between the transducers will not depend on the values of the parallel-connected resistances R_1 and R_2, we may assume that the expression (39) applies also to the transducers in the normal situation in which they are absent.

For numerical evaluation of transadmittance functions by means of (39), an expression for the source function $f(x, z)$ is required. In the weak-coupling approximation we assume that $f(x, z)$ may be obtained from the potential distribution ϕ_s and charge density σ_s on the underside of a finger, which arises in the solution for the electrostatic field when the given finger pattern is placed on an equivalent nonpiezoelectric substrate.

We make the further independent-gap approximation that the solution for the field in each gap (a gap is defined as the region between the electrical center of one finger at $z = z_k$, and the next at $z = z_{k+1}$, as shown in Fig. 5) is the same as we would obtain if that gap were part of an infinite length uniform width and spacing interdigital transducer. Taking the field of a uniform transducer obtained by Engan [10], we obtain the expression for $f(x, z)$ in the region $z_k < z < z_{k+1}$,

$$f(x,z) = \frac{\pi}{1.854(z_{k+1}-z_k)} \cdot \sum_{n=0}^{\infty}(-1)^n[(\epsilon_p/\epsilon_0)+(\beta/\beta_n)]P_n(0)\cos(\beta_n z') \quad (40)$$

where $z_{k+1} - z_k$ is the size of the gap in question, $\beta_n = (2n+1)\pi/(z_{k+1}-z_k)$, $z' = z - z_k$, and $P_n(0)$ is the Legendre function of the first kind of zero argument. This source function, on a material of moderate dielectric constant such as quartz, has at frequencies reasonably close to band center the approximate form also shown in Fig. 5. In numerical calculations of the behavior of transducers over anything other than extreme bandwidth ratios, only a limited number of terms of the series for each gap need be taken. In the calculations presented later, only the first term, $(n = 0)$, is retained, as the

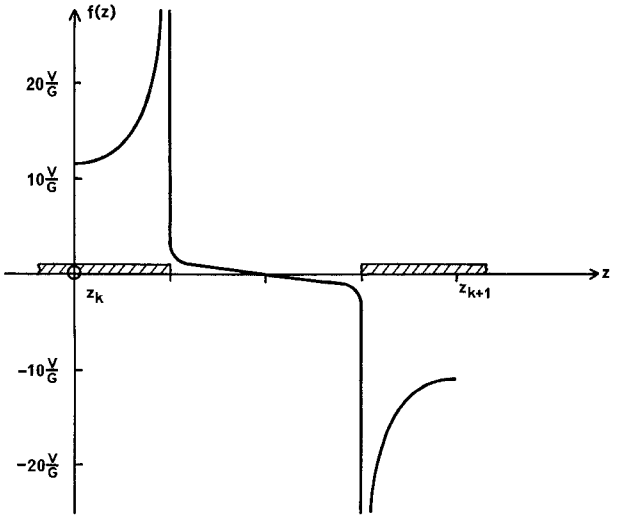

Fig. 5. Source function $f(z)$ for a uniform interdigital transducer on SiO_2, plotted between the centers of two adjacent electrodes spaced by a distance $G=z_{k+1}-z_k$. The regions $z_k \leq z \leq z_k+G/4$ and $z_{k+1}-G/4 \leq z \leq z_{k+1}$ are metallized.

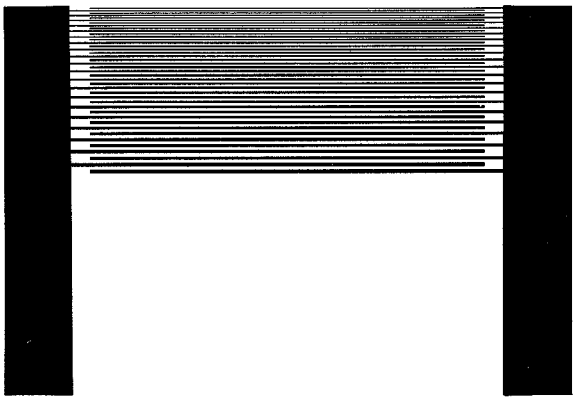

Fig. 6. Electrode pattern for one of the two frequency-chirped transducers used in the experimental wide-band delay line.

next nonzero term, $(n=2)$, has $\beta_2=5\beta_0$ and is considered as unlikely to produce significant coupling to waves of propagation vector β. On the further assumption that coupling to the Rayleigh wave comes largely from those areas of a transducer which have $\beta_n \approx \beta$, and noting that the second term in square brackets in (40) represents, even on moderate dielectric constant substrates, only a small correction to the major coupling term, we replace (β/β_n) by unity in that equation and obtain the approximate expression

$$f(x, z) = \frac{\pi}{1.854(z_{k+1} - z_k)} \sum_{n=0}^{\infty} \left[\frac{\epsilon_p + \epsilon_0}{\epsilon_0}\right] P_n(0) \cos \beta_n z' \quad (41)$$

which has been used as the basis of the calculations.

IV. Practical Application

To test the validity of the transadmittance integral formulation, the theory was used to predict the insertion loss and frequency response of a wide-band surface-wave filter, and the results were compared with an experimental measurement of the same parameters. The line used had identical frequency-chirped transducers at the input and output ports, one of which is shown in Fig. 6, and was fabricated using

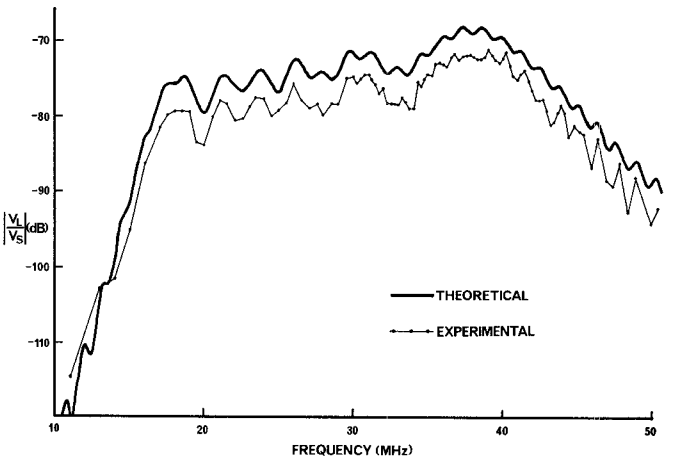

Fig. 7. Voltage transfer ratio for a wide-band surface-wave delay line utilizing an identical pair of unapodized logarithmically frequency-chirped transducers.

aluminum electrodes on YX-quartz. The 41 electrodes were unapodized and spaced so that the ratio of successive gap widths was held constant at 0.9722. This resulted in a ratio of the first gap width to the last gap width of 3.0; the synchronous frequencies for the first and last gaps were 15 and 45 MHz, respectively. The gap widths were arranged to be equal to half the sum of the two adjacent electrode widths at all points along the transducer. The electrode lengths were fixed at 4.7 mm, corresponding to 50λ at 33.5 MHz.

Both transducers were frequency-chirped in the same direction to give constant delay with frequency.

Theoretical Response

The predicted voltage transfer function was determined using a digital computer by first calculating $Y_{21}(\omega)$ as a function of frequency using (39) and then substituting in (4). In the computation, use was made of the fact that when the transducers are not apodized, the area integrals in (39) reduce to one-dimensional integrals which form, in fact, the familiar Fourier transform. These integrals were then evaluated separately using a 1024-point complex FFT algorithm.

Before this could be done, it was necessary to obtain a spatial representation of the source function $f(x, z)$. No attempt was made to model the harmonic response of the transducer on this occasion, and it was assumed that this would not seriously affect the passband response of the line. The next step involved the assumption that the source function in each gap is not greatly affected by the geometry of the adjacent gaps, and hence the source function in each gap would be identical to that expected in a uniform infinitely long transducer with the same gap width. In this way, a source function was assembled by assuming in each gap the waveform responsible for exciting the fundamental component corresponding to that gap (the word "gap" here refers to the region between the electrical centers of adjacent electrodes).

The calculated magnitude of the voltage transfer ratio $|Y_{21}Z_L|$, based on the above calculations for $Y_{21}(\omega)$ and measured values of $Z_L(\omega)$, is shown as the solid curve of Fig. 7.

Experimental Results

The delay line was mounted in a metal box with careful screening between the input and output wiring to minimize

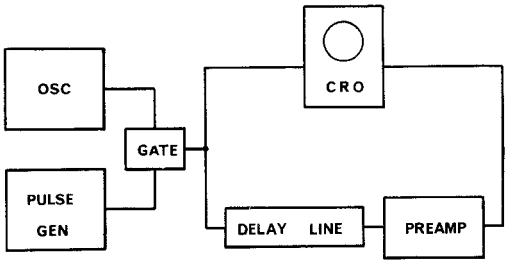

Fig. 8. Schematic of the delay line measurement circuit.

direct capacitive coupling of input signals to the output. The measurement system is shown in Fig. 8. All cables were 50-Ω characteristic impedance and were terminated in 50 Ω at the oscilloscope. The input impedance to the delay line was confirmed to be much higher than 50 Ω, and no attempt was made to tune or match the transducers.

Initially, short bursts of RF signal were used to excite the line to facilitate the identification of undesired propagating modes reaching the output transducer. As expected with such wide-band transducers, significant volume mode energy was reaching the receiving transducer at the higher frequencies. These modes were removed by cutting a number of slots into, and adding black wax to, the underside of the crystal.

The measurements were then performed using very long pulses, and the modulus of the voltage transfer ratio so obtained is shown as the experimental points in Fig. 7. It can be seen that the magnitudes of the theoretical and experimental voltage transfer ratios, neither of which contains adjustable constants, are in good agreement. The greater insertion loss in the experimental result can be attributed to resistive losses, diffraction, and the effects of slight pattern and crystal misalignment, which were not included in the calculations. A notable feature of the passband response is an approximate 6-dB rise between 17 and 37 MHz superimposed on the passband ripples. These features may be understood by observing that in the stationary phase approximation [11], integrals F_1 and F_2 (37), if carried out over transducers having a logarithmic gap taper and infinite length, are independent of frequency. The factor $|\omega|$ in the forward transadmittance expression then predicts a frequency response rising at 6 dB per octave. The passband ripples evident in Fig. 7 arise from the use of transducers of finite length, and in a practical device would be minimized by suitably tapering the electrode overlaps at each end of the transducer.

V. Conclusions

The admittance formulation has been shown to form a convenient basis for the calculation of many of the quantities of interest in tapped delay lines and one-port information stores. Existing formulations for the derivation of the input admittances of an N-port structure have been supplemented by a theory which provides explicit calculation procedures for the determination of the transadmittance between two transducers on a weak-coupling substrate.

Calculations of the transadmittance for a wide-band filter using approximate expressions for the potential and charge distributions show good agreement with experiment. There is some discrepancy between measured and theoretical results at higher frequencies, which is thought to arise from the use of the independent-gap approximation for the field and charge distributions, and may possibly also be related to the weak-coupling approximation.

References

[1] W. R. Smith *et al.*, "Analysis of interdigital surface wave transducers by use of an equivalent circuit model," *IEEE Trans. Microwave Theory Tech. (Special Issue on Microwave Acoustics)*, vol. MTT-17, pp. 856–864, Nov. 1969.
[2] B. A. Auld and G. S. Kino, "Normal mode theory for acoustic waves and its application to the interdigital transducer," *IEEE Trans. Electron Devices*, vol. ED-18, pp. 898–908, Oct. 1971.
[3] R. F. Milsom and M. Redwood, "Piezoelectric generation of surface waves by interdigital array," *Proc. Inst. Elec. Eng.* (London), vol. 118, pp. 831–840, July 1971.
[4] R. H. Tancrell and M. G. Holland, "Acoustic surface wave filters," *Proc. IEEE*, vol. 59, pp. 393–409, Mar. 1971.
[5] D. P. Morgan, "Log-periodic transducers for acoustic surface waves," *Proc. Inst. Elec. Eng.* (London), vol. 119, pp. 55–60, Jan. 1972.
[6] W. R. Smith, H. M. Gerard, and W. R. Jones, "Analysis and design of dispersive interdigital surface-wave transducers," *IEEE Trans. Microwave Theory Tech.*, vol. MTT-20, pp. 458–471, July 1972.
[7] W. S. Jones, C. S. Hartmann, and T. D. Sturdivant, "Second order effects in surface wave devices," *IEEE Trans. Sonics Ultrason.*, vol. SU-19, pp. 368–377, July 1972.
[8] B. A. Auld, "Surface wave theory," in *Proc. 1970 IEEE Ultrason. Symp.* New York: IEEE, 1971, pp. 1–15.
[9] K. A. Ingebrigtsen, "Surface waves in piezoelectrics," *J. Appl. Phys.*, vol. 40, pp. 2681–2686, June 1969.
[10] H. Engan, "Excitation of elastic surface waves by spatial harmonics of interdigital transducers," *IEEE Trans. Electron Devices*, vol. ED-16, pp. 1014–1017, Dec. 1969.
[11] C. E. Cook and M. Bernfeld, *Radar Signals.* New York: Academic Press, 1967, p. 34.